
AFRL-AFOSR-VA-TR-2020-0141

# Discontinuous Petrov Galerkin (DPG) Solvers for Maxwell Equations and Related Wave Propagation Problems

**Leszek Demkowicz**
**UNIVERSITY OF TEXAS AT AUSTIN**

**08/03/2020**
**Final Report**



Air Force Research Laboratory
AF Office Of Scientific Research (AFOSR)/ RTA2
Arlington, Virginia 22203
Air Force Materiel Command

# REPORT DOCUMENTATION PAGE

*Form Approved*
*OMB No. 0704-0188*



| 1. REPORT DATE *(DD-MM-YYYY)* | 2. REPORT TYPE | 3. DATES COVERED *(From - To)* |
|---|---|---|
| 18-08-2020 | Final Performance | 15 Dec 2016 to 14 Dec 2019 |

**4. TITLE AND SUBTITLE**
Discontinuous Petrov Galerkin (DPG) Solvers for Maxwell Equations and Related Wave Propagation Problems

**5a. CONTRACT NUMBER**

**5b. GRANT NUMBER**
FA9550-17-1-0090

**5c. PROGRAM ELEMENT NUMBER**
61102F

**6. AUTHOR(S)**
Leszek Demkowicz, S. Gopalakrishnan

**5d. PROJECT NUMBER**

**5e. TASK NUMBER**

**5f. WORK UNIT NUMBER**

**7. PERFORMING ORGANIZATION NAME(S) AND ADDRESS(ES)**
UNIVERSITY OF TEXAS AT AUSTIN
110 INNER CAMPUS DR, MN 13
AUSTIN, TX 78712 US

**8. PERFORMING ORGANIZATION REPORT NUMBER**

**9. SPONSORING/MONITORING AGENCY NAME(S) AND ADDRESS(ES)**
AF Office of Scientific Research
875 N. Randolph St. Room 3112
Arlington, VA 22203

**10. SPONSOR/MONITOR'S ACRONYM(S)**
AFRL/AFOSR RTA2

**11. SPONSOR/MONITOR'S REPORT NUMBER(S)**
AFRL-AFOSR-VA-TR-2020-0141

**12. DISTRIBUTION/AVAILABILITY STATEMENT**
A DISTRIBUTION UNLIMITED: PB Public Release

**13. SUPPLEMENTARY NOTES**

**14. ABSTRACT**
he primary goal of this project is to build fast tools for simulating optical ber ampliers and apply them to enhance our understanding of Transverse Mode Instability (TMI). TMI is currently the main roadblock preventing further power scaling of ber ampliers.

**15. SUBJECT TERMS**
Petrov-Galerkin, wave propagation

| 16. SECURITY CLASSIFICATION OF: | | | 17. LIMITATION OF ABSTRACT | 18. NUMBER OF PAGES | 19a. NAME OF RESPONSIBLE PERSON |
|---|---|---|---|---|---|
| a. REPORT | b. ABSTRACT | c. THIS PAGE | | | FAHROO, FARIBA |
| Unclassified | Unclassified | Unclassified | UU | | 19b. TELEPHONE NUMBER *(Include area code)* 703-696-8429 |

Standard Form 298 (Rev. 8/98)
Prescribed by ANSI Std. Z39.18

| | |
|---|---|
| *Title:* | DISCONTINUOUS PETROV GALERKIN (DPG) SOLVERS FOR MAXWELL EQUATIONS AND RELATED WAVE PROPAGATION PROBLEMS |
| *Investigators:* | LESZEK DEMKOWICZ & JAY GOPALAKRISHNAN |
| *AFRL Collaborator:* | JACOB GROSEK |
| *Program Officers:* | JEAN-LUC CAMBIER, FARIBA FAHROO |
| *Program:* | COMPUTATIONAL MATHEMATICS |

## Goals of the project.

- Create efficient robust multilevel DPG Maxwell solvers for high frequency wave propagation.
  **Approach:** Integrate multilevel solver techniques with local adaptive refinement guided by DPG error estimators.

- Simulate nonlinear optical effects in high power laser fiber amplifiers in collaboration with AFRL.
  **Approach:** Build a hierarchy of optical fiber models, from full-featured Maxwell system to coupled mode approximations.

# 1 Research Accomplishments

## 1.1 Hierarchy of models

The basic configuration modeled consists of a fiber "core" region and outer regions. A schematic of a standard double-clad step-index fiber can be seen in Figure 1. A physical fiber usually also includes an outer polymer coating. In all considered configurations, there is a defined "core" region where most of the energy is guided. In a fiber amplifier, the core is seeded by a continuous wave input of highly coherent laser light, typically called the "signal". Simply put, we are interested in how the signal light is amplified by energy transfer from "pump" light while it propagates through the fiber, through the process called "gain".

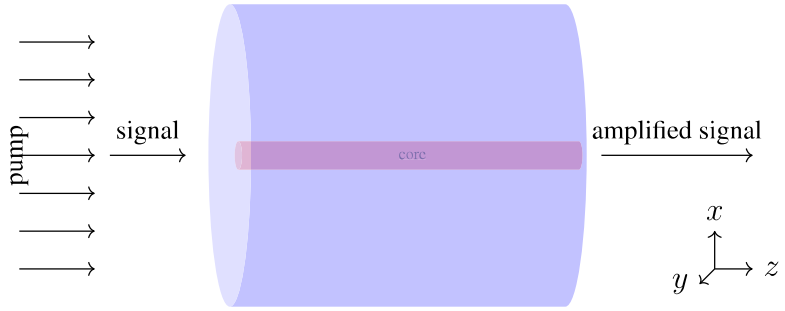


Figure 1: Schematic of a single-clad fiber amplifier; a double-clad amplifier would have an additional polymer coating around the cladding shown above.

We have been working with a hierarchy (see Figure 2) of progressively reduced models, which we now shortly explain. Our suite of models begins with the Maxwell system for both pump and

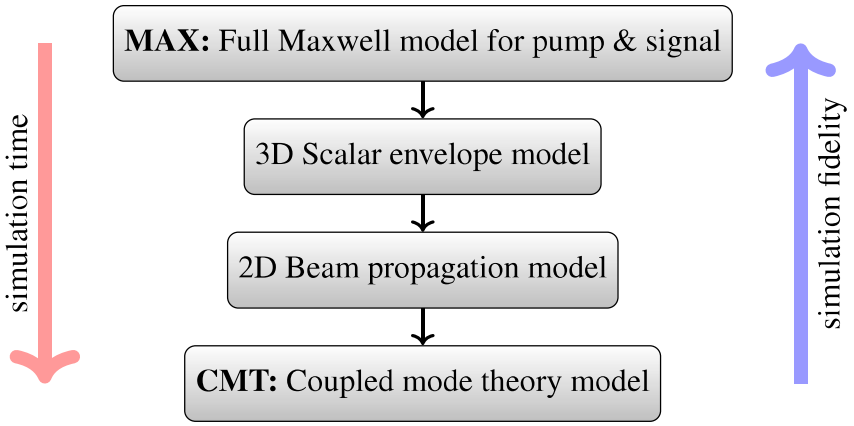


Figure 2: Hierarchy of models

signal. Assume that the electromagnetic fields (signal and pump) are time harmonic of frequencies $\omega_s$ and $\omega_p$, respectively. We postulate that the signal field $\vec{E}_s, \vec{H}_s$ and the pump field $\vec{E}_p, \vec{H}_p$, independently satisfy Maxwell equations, but are coupled through polarization terms, i.e.,

$$\operatorname{curl} \vec{E}_\ell - \hat{\imath}\omega_\ell \mu_0 \vec{H}_\ell = 0, \qquad \operatorname{curl} \vec{H}_\ell + \hat{\imath}\omega_\ell \epsilon_0 \vec{E}_\ell = -\hat{\imath}\omega_\ell \vec{P}_\ell, \qquad \ell \in \{s, p\}, \tag{1.1}$$

where $\epsilon_0$ is the electric permittivity and $\mu_0$ is the vacuum magnetic permeability. All interactions of light with matter are modeled through the polarization terms of the form

$$\vec{P}_\ell = \underbrace{\vec{P}^{\text{bg}}(\vec{E}_\ell)}_{\substack{\text{background}\\ \text{polarization}}} + \underbrace{\vec{P}^{\text{ag}}(\vec{E}_s, \vec{E}_p)}_{\substack{\text{active}\\ \text{gain}}} + \underbrace{\vec{P}^{\text{rg}}(\vec{E}_s, \vec{E}_p)}_{\substack{\text{Raman}\\ \text{gain}}} + \underbrace{\vec{P}^{\text{th}}(\vec{E}_s, \vec{E}_p)}_{\substack{\text{thermal}\\ \text{effects}}} + \underbrace{\cdots}_{\substack{\text{other optical}\\ \text{nonlinearities}}}$$

The linear background polarization is textbook material: $\vec{P}^{\text{bg}}_\ell(\vec{E}_\ell) = \epsilon_0(n^2 - 1)\vec{E}_\ell$ where $n$ is the refractive index of the medium. We model the active gain polarization by $\vec{P}^{\text{ag}}_\ell(\vec{E}_s, \vec{E}_p) = -\hat{\imath}\epsilon_0 n(c/\omega_\ell) g_\ell \vec{E}_\ell$, where c is the speed of light and $g_\ell \equiv g_\ell(\vec{E}_s, \vec{E}_p)$ is the *active gain term that depends on* $\vec{E}_s, \vec{E}_p$ *in some nonlinear* fashion, depending on the medium.

Examples of $g_\ell$ we have in mind are expressed in terms of the irradiance $I_\ell = n|\vec{E}_\ell|^2/\mu_0 c$. Light of high irradiance can perturb the refractive index causing many interesting nonlinear effects in optical fibers, such as in Example 1.1 below. However, of primary interest to us in the simulation of fiber amplifiers is *active gain*, occurring in fibers whose core is doped with lanthanide rare-earth metallic elements, such as Thulium (Tm) or Ytterbium (Yb) – see Example 1.2. They result in much larger gain due to the pump light driving dopant ions to excited radiative states followed by stimulated emission into signal photons.

**Example 1.1** (Raman gain)**.** As described in [16, 22], the nonlinear Raman gain can be modeled using a measurable "bulk Raman gain coefficient" $g_R$ by

$$g_\ell = \Upsilon_\ell g_R I_{\ell^c}, \qquad \ell \in \{s, p\} \tag{1.2}$$

where $\Upsilon_p = -\omega_p/\omega_s$, $\Upsilon_s = 1$, and $\ell^c \in \{s, p\} \setminus \{\ell\}$, the complementary index of $\ell$. □

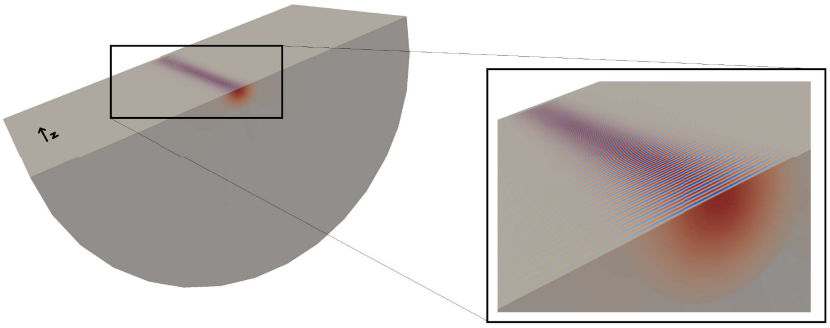

Figure 3: A simulation from [16] using the MAX model

**Example 1.2** (Ytterbium-doped fiber)**.** Yb-doped fiber amplifiers are usually pumped at $\lambda_p$ =976 nm to move ions from a ground state (manifold ${}^2F_{7/2}$) to an excited state (manifold ${}^2F_{5/2}$) [9, 17]. After undergoing a rapid non-radiative transition to a lower energy state, the amplifier can lase around $\lambda_s$ =1064 nm very efficiently. Denoting the ion population as $N_{\text{total}} = N_{\text{excited}} + N_{\text{ground}}$, the active gain can be modeled by

$$g_\ell = \sigma_\ell^{\text{ems}} N_{\text{excited}} - \sigma_\ell^{\text{abs}} N_{\text{ground}} = N_{\text{total}} \big[\sigma_\ell^{\text{ems}} \varepsilon - \sigma_\ell^{\text{abs}} (1-\varepsilon)\big] \tag{1.3}$$

where the excited ion fraction $\varepsilon = N_{\text{excited}}/N_{\text{total}}$ is calculated in terms of a radiative lifetime ($\tau$), and absorption and emission cross sections ($\sigma_\ell^{\text{abs}}, \sigma_\ell^{\text{ems}}$) as $\varepsilon = c^{\text{abs}}/(c^{\text{abs}} + c^{\text{ems}} + \tau^{-1})$, where $c^{\text{e/a}} = \sigma_p^{\text{e/a}} I_p/\hbar\omega_p + \sigma_s^{\text{e/a}} I_s/\hbar\omega_s$, for $\text{e/a} \in \{\text{ems}, \text{abs}\}$ and $\omega_\ell = 2\pi c/\lambda_\ell$. □

Using a gain function $g_\ell$ as in the above examples, with appropriate boundary conditions, we have completed the description of the *MAX Model*, the top model in the hierarchy indicated in Figure 2. Our preliminary numerical experience with this model using Raman gain has been detailed in [16] (see also Figure 3).

A starting point to obtain further simplified models is the elimination of $\vec{H}_\ell$ from (1.1), to obtain the second order equation $\operatorname{curl}\operatorname{curl}\vec{E}_\ell - \omega_\ell^2\epsilon_0\mu_0\vec{E}_\ell = \omega_\ell^2\mu_0\vec{P}_\ell$ for the electric field alone. For ease of exposition, let us now focus only on the case of active gain polarization (although other types of polarization terms can be similarly incorporated). Substituting $\vec{P}_\ell = \vec{P}_\ell^{\text{bg}} + \vec{P}_\ell^{\text{ag}} = \epsilon_0(n^2-1)\vec{E}_\ell - \frac{\hat{\imath}\epsilon_0 cn}{\omega_\ell} g_\ell \vec{E}_\ell$, using $c = 1/\sqrt{\epsilon_0\mu_0}$, and simplifying, we get,

$$\operatorname{curl}\operatorname{curl}\vec{E}_\ell - k_\ell^2 n^2 \vec{E}_\ell + \hat{\imath} k_\ell n g_\ell \vec{E}_\ell = 0, \tag{1.4}$$

where $k_\ell = \omega_\ell/c$ is the wavenumber corresponding to the frequency $\omega_\ell$. The next simplification is to assume that the electric field $\vec{E}_\ell$ can be expressed as $\vec{E}_\ell(x,y,z) = U_\ell(x,y,z)\hat{e}_x$, i.e., it is linearly polarized in a fixed transverse direction, which is taken above to be the $x$-direction (where $\hat{e}_x$ denotes the unit vector in the $x$-direction). Furthermore, since $\vec{E}_\ell$ has high frequency oscillations along the $z$-direction, its variations along the transverse directions may be considered negligible. It is therefore standard in optics to neglect $\operatorname{grad}\operatorname{div}\vec{E}_\ell$. These assumptions imply that the vector equation (1.4) becomes the following scalar Helmholtz equation for $U_\ell$,

$$-\Delta U_\ell - k_\ell^2 n^2 U_\ell + \hat{\imath} k_\ell n g_\ell U_\ell = 0. \tag{1.5}$$

Due to the high wave number $k_\ell$, even this simplified problem is computationally intensive, so we seek even further simplified models. All models other than the MAX model in Figure 2 are derived from (1.5). The scalar envelope model is derived from (1.5) by assuming that $U_\ell(x, y, z)$ can be expressed as $A(x, y, z)e^{\hat{\imath}\beta z}$ for some $\beta$ close to an effective propagation constant. This makes $A$ more slowly varying than $U$ and leads to a tractable scalar 3D model. If one is further willing to neglect $\partial_{zz}A$, then it is possible to make a further simplification from 3D to a 2D model that can solved for by stepping through the fiber, akin to a time stepping scheme. This is often called BPM, or the Beam Propagation Method. We have experimented with all these models. The main focus, however, has been on top and bottom models in Figure 2, namely the MAX model, and the CMT (Coupled Mode Theory) model, which we now shortly describe.

The CMT model uses the *transverse core modes* of the fiber to construct an electric field ansatz. These modes $\varphi_l(x, y)$ are non-trivial functions that, together with their accompanying (positive) *propagation constants* $\beta_l$, solve the eigenproblem

$$(\Delta_{xy} + k_s^2 n^2)\varphi_l = \beta_l^2 \varphi_l, \tag{1.6}$$

where $\Delta_{xy} = \partial_{xx} + \partial_{yy}$ denotes the transverse Laplacian. The guided modes decay exponentially in the cladding region. There can only be finitely many such modes, which we index using $l = 1, 2, \ldots, M$. For step-index fibers, these modes are called the linearly polarized (LP) transverse guided core modes [1]. The mode-based field ansatz is

$$U_s(x, y, z) = \sum_{m=1}^{M} A_m(z)\varphi_m(x, y)e^{\hat{\imath}\beta_m z}. \tag{1.7}$$

The ansatz (1.7) reduces the field computation to the computation of $A_l(z)$. If $A_m$ is so slowly varying in $z$ that we neglect $d^2A_m/dz^2$, then substituting (1.7) into (1.5) and simplifying using the $L^2$ orthogonality of the modes, we find that $A_l$ satisfies the system of ordinary differential equations (ODE)

$$\frac{dA_l}{dz} = \sum_{m=1}^{M} e^{\hat{\imath}(\beta_m - \beta_l)z}\, K_{lm}(A, I_p)\, A_m, \qquad 0 < z < L, \tag{1.8}$$

for $l = 1, \ldots, M$, where the mode coupling coefficient $K_{lm}$ is given by

$$K_{lm}(A, I_p) = \frac{k_s}{2\beta_l} \int_{\Omega_z} g_s(I_s(x, y, A), I_p)\, n(x, y)\varphi_m(x, y)\overline{\varphi_l(x, y)}\, dx\, dy. \tag{1.9}$$

Here $\Omega_z$ represents the fiber cross section having the constant longitudinal coordinate value of $z$. Equation (1.8) when combined with an even more simplified model of pump irradiance $I_p$, are the equations of the CMT model. More details on this and our preliminary computational experiences with the CMT model can be found in [7].

## 1.2 Fast DPG Maxwell solvers for the MAX model

This and the next two subsections (§§1.2–1.2.2) summarize the work on higher order *Discontinuous Petrov-Galerkin (DPG)* solvers for the MAX model, which is based on (1.1). To account for the

thermal effects, the two sets of Maxwell equations are weakly coupled with the transient heat equation as in [13]. The time scales for the heat and Maxwell equations differ by three orders of magnitude and this dictates the overall structure of the final algorithm. We use the simplest implicit Euler method to discretize the heat equation. The heat source is calculated from the energy deposited by both pump and signal waves. In turn, the refractive index in the Maxwell system is a function of the temperature. The weak coupling means that we freeze temperature when we solve for the EM fields and we freeze EM fields when we solve for the temperature. Within the single time step of the heat equation (milliseconds), the Maxwell equations reach a steady state which explains why we can use the time-harmonic Maxwell equations. The pump/signal Maxwell system is currently solved using simple iterations though more sophisticated nonlinear methods are possible as well.

Next, we decsribe the Maxwell solver and discuss its three essential components. We begin with a short description of mathematical foundations behind the DPG methodology in the next few paragraphs, report on successful modeling of lasing using the Raman model in §1.2.2, and in §1.2.3 outline the work on fast Maxwell solvers. The work consists of both numerical analysis and advanced software development and the latter has so far proceeded within the OpenMP version of the *hp3D* code. The discretization method we use for the Maxwell system is the specific variant of the DPG method described next.

### 1.2.1 The ultraweak DPG method

The original development of the DPG method [3] took place within the context of *ultraweak variational formulation*. In time, we learned that the technology of broken test spaces and optimal test functions can be applied within the framework of any well-posed variational problem but the ultraweak DPG method remains special. There are at least three good reasons for that.

*1. The most relaxed functional setting.* Derivation of the ultraweak variational formulation starts with the first-order system:

$$\begin{cases} \mathsf{u} \in D(A) \\ A\mathsf{u} = \mathsf{f} \qquad \text{in } L^2(\Omega) \end{cases} \tag{1.10}$$

where $\mathsf{u}$ represents a group variable, $A$ stands for the operator corresponding to the system of first-order PDEs, and $D(A)$ denotes the domain of the operator incorporating the BCs. For instance, for the linear Maxwell equations, we have:

$$\mathsf{u} = \begin{bmatrix} E \\ H \end{bmatrix}, \quad A \begin{bmatrix} E \\ H \end{bmatrix} = \begin{bmatrix} i\omega\epsilon & -\text{curl} \\ \text{curl} & i\omega\mu \end{bmatrix} \begin{bmatrix} E \\ H \end{bmatrix} = \begin{bmatrix} i\omega\epsilon E - \text{curl} H \\ \text{curl} E + i\omega\mu H \end{bmatrix}$$

and, in the case of perfect conductor boundary, $D(A) := \{(E,H) \in \vec{L}^2(\Omega) : A(E,H) \in \vec{L}^2(\Omega),\ n \times E = 0 \text{ on } \Gamma\}$ where $\vec{L}^2(\Omega) := (L^2(\Omega))^N \times (L^2(\Omega))^N$. The ultraweak variational formulation is obtained by multiplying both sides of the equation with a test function $\mathsf{v} \in D(A^*)$. Integrating by parts and utilizing the boundary conditions, we obtain

$$\begin{cases} \mathsf{u} \in \vec{L}^2(\Omega) \\ (\mathsf{u}, A^*\mathsf{v}) = (\mathsf{f}, \mathsf{v}) \quad \mathsf{v} \in D(A^*) \end{cases} \tag{1.11}$$

*2. Robust stability.* With $\mathsf{v}$ controlled in the adjoint norm, termed *the optimal test norm* $\|\mathsf{v}\|_{opt} = \|A^*\mathsf{v}\|$ the bilinear form becomes a duality pairing, and the corresponding ideal Petrov-Galerkin discretization with optimal test functions delivers $L^2$-projection. Unfortunately, the adjoint norm is not *localizable* and cannot be used in DPG implementation. However, if the original operator is bounded below with a constant $\gamma$,

$$\|A\mathsf{u}\| \geq \gamma\|\mathsf{u}\|, \quad \mathsf{u} \in D(A) \qquad \Leftrightarrow \qquad \|A^*\mathsf{v}\| \geq \gamma\|\mathsf{v}\|, \quad \mathsf{v} \in D(A^*)\,,$$

then the adjoint norm is equivalent to the localizable *adjoint graph norm*, $\|\mathsf{v}\|_V^2 = \|A^*\mathsf{v}\|^2 + \alpha^2\|\mathsf{v}\|^2$ . As the adjoint and the adjoint graph norms are equivalent,

$$\|A^*\mathsf{v}\|^2 \leq \|A^*\mathsf{v}\|^2 + \alpha^2\|\mathsf{v}\|^2, \qquad \|A^*\mathsf{v}\|^2 + \|\mathsf{v}\|^2 \leq \left(1 + \frac{\alpha^2}{\gamma^2}\right)\|A^*\mathsf{v}\|^2,$$

the ideal DPG method corresponding to the adjoint graph test norm delivers an orthogonal projection in a norm equivalent to the $L^2$-norm. Of particular importance are *singular perturbation problems* with $\gamma$ being independent of the perturbation parameter. The DPG methodology delivers then a *robust* discretization.

Finally, testing with the larger class of discontinuous or *broken* test functions, we obtain the ultimate variational formulation in the form:

$$\begin{cases} \mathsf{u} \in \vec{L}^2(\Omega), \hat{\mathsf{u}} \in H_A(\Gamma_h) \\ (\mathsf{u}, A^*\mathsf{v}) + \langle \hat{\mathsf{u}}, \mathsf{v}\rangle_{\Gamma_h} = (\mathsf{f}, \mathsf{v}) \quad \mathsf{v} \in H_{A^*}(\Omega_h) \end{cases} \tag{1.12}$$

in appropriately defined space $H_A(\Gamma_h)$ – see e.g., the general treatment in [6, Appendix]. The broken variational formulation retains optimal stability properties of unbroken ultraweak variational formulation with the adjoint graph test norm in terms of original unknown field $\mathsf{u}$. The extra unknown – the trace $\hat{\mathsf{u}}$ – lives on the mesh skeleton in the *trace energy space* corresponding to the strong form of the operator, and it is controlled in the *minimum energy extension norm*:

$$\|\hat{\mathsf{u}}\|^2 = \inf_{\mathsf{U}\in H_A(\Omega_h),\ \mathrm{tr}_{\Gamma_h}\mathsf{U}=\hat{\mathsf{u}}} \|A\mathsf{U}\|^2 + \|\mathsf{U}\|^2\,.$$

*3. Optimal spectral properties.* Being a minimum residual method, DPG always delivers a Hermitian positive definite stiffness matrix even if the original differential operator is indefinite. Therefore, the spectrum lies on the positive real axis. For wave propagation problems, the ultraweak DPG delivers stiffness matrices with best spectral properties [26]. The method has better dispersion properties than standard Galerkin but it is more diffusive. Nevertheless, it is the least diffusive version of the minimum residual methods.

### 1.2.2 Simulation of lasing using the Raman model

The coding challenges in simulating the MAX model for many wavelengths are manifold. As *all* methods suffer from numerical pollution in the high-frequency regime [2], it is essential to control such dispersion and diffusion errors. This comes at substantial computational cost, and it is here that high-order ($p \geq 5$) elements are absolutely critical to the success of the simulation. On the one hand, it is necessary to resolve each wavelength (e.g., at least two elements per wavelength);

but then, polynomial order must be increased to control numerical pollution errors. As mentioned previously, the ultraweak formulation suffers the least from numerical pollution effects among the various DPG formulations. It is therefore the method of choice in our simulation efforts. We have found that $p = 5$ is both sufficient and necessary to obtain accurate results up to 100 wavelengths [16, 15], assuming few (2-4) elements per wavelength. Preliminary results point towards a need in increasing $p$ further as we approach 1000 wavelengths and more.

Additionally, we have employed many advanced techniques within the *hp3D* framework, all of which are critical in enabling the MAX model simulations. The code supports curvilinear geometries—we use isoparametric elements of high order to capture the fiber geometry accurately; the nature of the MAX model requires support of complex multiphysics variables, and in the case of ultraweak DPG, we in fact make use of the *entire* exact sequence:

| | | | |
|---|---|---|---|
| Temperature field: | $H^1(\Omega_h)$ | Electromagnetic fluxes: | $H(\text{curl}\,, \Gamma_h)$ |
| Heat flux: | $H(\text{div}, \Gamma_h)$ | Electromagnetic fields: | $L^2(\Omega_h)$. |

Furthermore, the code supports elements of "all shapes" [12]: tetrahedra, hexahedra, prisms, and pyramids; after initially modeling the fiber core with prisms, we are now employing hexahedra which enables fast integration via sum factorization, accelerating the simulation by more than an order of magnitude [12, 15]. Further recent improvements to the *hp3D* framework included the coding of flux variable routines to exploit the nature of interface variables that do not have degrees of freedom in the interior of an element, as well as element-local static condensation routines eliminating interior degrees of freedom from the linear system via a Schur complement technique in parallel, leaving a much smaller global interface problem to be solved. For the global solve, we have in place interfaces to state-of-the-art direct solvers (MUMPS, PARDISO), in addition to our own multigrid preconditioned conjugate gradient solver described in §1.2.3. Lastly, the anisotropic $hp$-adaptive capabilities of the code have not been exploited in the MAX model simulations yet, but we are expecting to use them within the DPG framework to accurately capture local features of the nonlinear solution, including TMI. The entire code is OpenMP enabled and has showed near-optimal scalability on modern manycore architectures (e.g., Skylake (SKX) compute nodes).

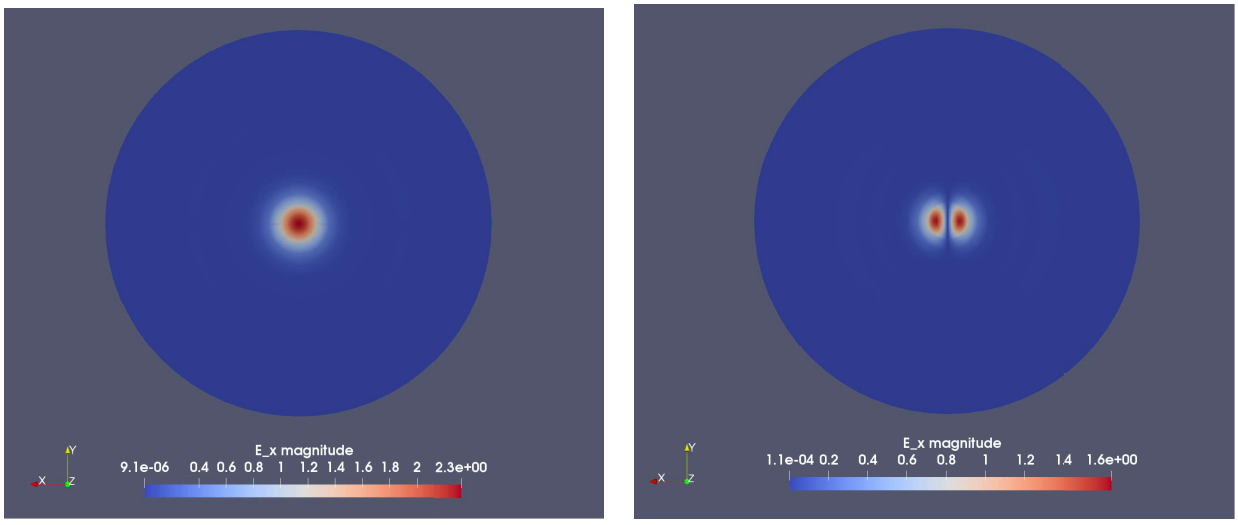


(a) $\text{LP}_{01}$ mode. (b) $\text{LP}_{11}$ mode.

Figure 4: LP modes propagating in weakly guiding step-index fiber.

Within the described framework, we have been able to accurately simulate propagation of various LP modes in single- and multi-mode weakly guiding step-index fibers. It has also been validated that the energy of propagating modes is confined to the core as predicted by Helmholtz analysis. To obtain correct results for multiple propagating modes, it was essential to model the fiber end with a perfectly matched layer (PML) instead of simpler impedance boundary condition [21, 16].

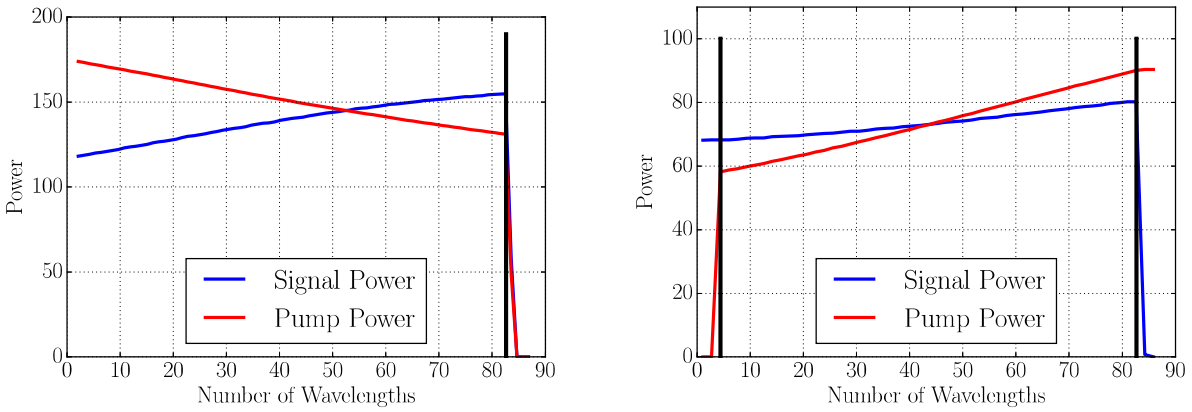


(a) Power in co-pumped configuration.

(b) Power in counter-pumped configuration.

Figure 5: Signal and pump power along fiber with Raman gain.

The nonlinear Maxwell model with Raman gain has successfully been implemented, simulating the transfer of energy from the pump field to the signal field for about 80 wavelengths, as shown in Figure 3 [16, 15]. With the MAX model, it is possible to model both co-pumped and counter-pumped configurations (cf. Figure 5), a capability that many other models do not possess. The temperature field and time-stepping from the heat equation has already been implemented, but studying effects of the heating on the electromagnetic fields of the propagating modes is ongoing work, and it will likely require considering substantially more wavelengths posing additional coding challenges.

### 1.2.3 DPG multigrid preconditioners for $hp$-meshes

In three-dimensional wave problems, especially in the high-frequency regime, very fine discretizations are needed in order to control both the best approximation error and the pollution effect [2, 4]. This often leads to prohibitively large linear systems which are very hard to solve. For simulations where the solution is localized, one can benefit from adaptive refinement strategies. The DPG method, with its unconditional discrete stability and its built-in error indicator, is a very powerful tool for such problems. In addition, the efficiency of the DPG adaptive method can be enhanced by employing iterative solvers to drive the adaptive refinements. In particular, throughout the $hp$-adaptive procedure, one is not interested in a fully converged solution on every mesh but only in a solution which is accurate enough to mark elements for refinement.

We have developed a novel adaptive geometric multigrid (MG) preconditioner for the Conjugate Gradient (CG) solver and we have integrated it within the adaptive process. Recall, that the

use of the ultraweak formulation allows for the interior degrees of freedom to be eliminated in an element-wise fashion, resulting in a linear system of significantly reduced size, that involves only interface unknowns. With a special construction of inter-grid transfer operators based on Schur complements, the preconditioner can operate on trace variables defined on the mesh skeleton. The preconditioner has been successfully applied for the solution of large problems in acoustics and electromagnetics, problems that where impossible to solve with direct solvers (see Figures 6 and 7). A more detailed discussion on the construction can be found in [26] for the two dimensional acoustics problem . An extension to three space dimensions for both acoustics and Maxwell equations, along with some theoretical convergence results can be found in [19].

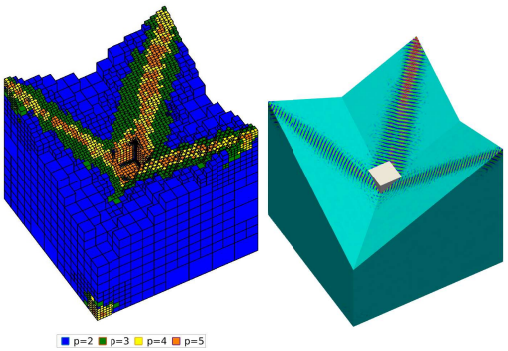


Figure 6: Acoustics: High frequency beam scattering from a cube. On the left: the $hp$ adaptive mesh. On the right: the numerical pressure.

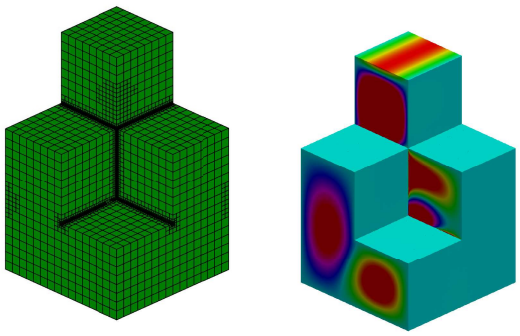

Figure 7: Electromagnetics - Fichera 'oven' problem. On the left: the $h$-adaptive mesh. On the right: the $x$-component of the electric field.

# References


[1] G. P. Agrawal. *Nonlinear Fiber Optics*. Elsevier, fifth edition, 2013.

[2] I. M. Babuška and S. A. Sauter. Is the pollution effect of the FEM avoidable for the Helmholtz equation considering high wave numbers? *SIAM Rev.*, 42(3):451–484 (electronic), 2000.

[3] L. Demkowicz and J. Gopalakrishnan. A class of discontinuous Petrov-Galerkin methods. Part II: Optimal test functions. *Numerical Methods for Partial Differential Equations*, 27(1):70–105, 2011.

[4] L. Demkowicz, J. Gopalakrishnan, I. Muga, and J. Zitelli. Wavenumber explicit analysis for a DPG method for the multidimensional Helmholtz equation. *Computer Methods in Applied Mechanics and Engineering*, 213/216:126–138, March 2012.

[5] L. Demkowicz, J. Gopalakrishnan, S. Nagaraj, and P. Sepulveda. A spacetime DPG method for the Schrödinger equation. *SIAM J. Numer. Anal.*, 55(4):1740–1759, 2017.

[6] T. Ehrenreich, R. Leveille, I. Majid, K. Tankala, G. Rines, and P. Moulton. 1-kW, All-Glass Tm: fiber Laser. In *Proc. SPIE*, vol. 7580, p. 758016, 2010.

[7] J. Gopalakrishnan, T. Goswami, and J. Grosek. *Techniques for modeling fiber laser amplifiers.* Submitted to Proc. SCEE (extended abstract of a plenary talk), Taormina, Italy, 2018

[8] J. Gopalakrishnan, L. Grubišić, and J. Ovall. Spectral discretization errors in filtered subspace iteration. *Preprint: arXiv:1709.06694*, 2018.

[9] J. Grosek, S. Naderi, B. Oliker, R. Lane, I. Dajani, and T. Madden. Laser simulation at the Air Force Research Laboratory. In *Proc. SPIE*, vol. 10254, p. 102540N-1, 2017.

[10] C. Jauregui, T. Eidam, J. Limpert, and A. Tünnermann. The impact of modal interference on the beam quality of high-power fiber amplifiers. *Opt. Express* 19(4):3258–3271, 2011.

[11] C. Jauregui, J. Limpert, and A. Tünnermann. High-power fibre lasers. *Nature Photonics*, 7(11):861–867, 2013.

[12] J. Mora and L. Demkowicz. Fast integration of DPG matrices based on tensorization. *Computational Methods in Applied Mathematics*, 19(3):523–555, 2019.

[13] S. Naderi, I. Dajani, J. Grosek, and T. Madden. Theoretical and numerical treatment of modal instability in high-power core and cladding-pumped Raman fiber amplifiers. *Optics Express*, 24(15):16550–16565, 2016.

[14] S. Naderi, I. Dajani, T. Madden, and C. Robin. Investigations of modal instabilities in fiber amplifiers through detailed numerical simulations. *Optics Express*, 21(13):16111–16129, 2013.

[15] S. Nagaraj. *DPG methods for nonlinear fiber optics*. PhD thesis, 2018.

[16] S. Nagaraj, J. Grosek, S. Petrides, L. Demkowicz, and J. Mora Paz. A 3d DPG Maxwell approach to nonlinear Raman gain in fiber laser amplifiers. *J. Comp. Phys.*, 2019. First published version available online: 9-MAR-2019 DOI information: 10.1016/j.jcpx.2019.100002.

[17] H. Pask, R. Carman, D. Hanna, A. Tropper, C. Mackechnie, P. Barber, and J. Dawes. Ytterbium-doped silica fiber lasers: versatile sources for the 1-1.2 $\mu$m region. *IEEE Journal of Selected Topics in Quantum Electronics*, 1(1):2–13, May 1995.

[18] S. Petrides and L. Demkowicz. An Adaptive DPG Method for High Frequency Time-harmonic Wave Propagation Problems. *Comput. Math. Appl.* 74(8):1999–2017, 2017.

[19] S. Petrides and L. Demkowicz. Multilevel solvers for the DPG method with applications in acoustics and electromagnetics. *ICES report (in preparation)*.

[20] R. Scarmozzino, A. Gopinath, R. Pregla, and S. Helfert. Numerical Techniques for Modeling Guided-Wave Photonic Devices. *IEEE Journal of Selected Topics in Quantum Electronics*, 6(1:)150–162, 2000.

[21] A. Vaziri, B. Keith, and L. Demkowicz. On perfectly matched layers for discontinuous Petrov-Galerkin methods. *arXiv preprint arXiv:1804.04496*, 2018.

[22] J. T. Verdeyen. *Laser electronics*. Prentice Hall, 3 edition, 1995.

# 2 Publications Supported with the Project

# References


[1] J. Badger, S. Henneking, and L. Demkowicz. Fast integration of DPG matrices based on tensorization (Part II: Prismatic elements). *Finite Elements in Analysis & Design*, 172:103385, 2020. accepted.

[2] Andrew T. Barker, Veselin Dobrev, Jay Gopalakrishnan, and Tzanio Kolev. A scalable preconditioner for a DPG method. *SIAM J. Sci. Comput.*, 40(2):A1187–A1203, 2018.

[3] L. Demkowicz, T. Fuehrer, N. Heuer, and X. Tian. The double adaptivity paradigm (How to circumvent the discrete inf-sup conditions of Babuška and Brezzi). Technical Report 7, Oden Institute, May 2019. Comp. Math. Appl., revised version in review.

[4] L. Demkowicz and J. Gopalakrishnan. *Encyclopedia of Computational Mechanics, Second Edition*, chapter Discontinuous Petrov-Galerkin (DPG) Method. Wiley, 2018. Eds. Erwin Stein, René de Borst, Thomas J. R. Hughes, see also ICES Report 2015/20.

[5] L. Demkowicz, J. Gopalakrishnan, and B. Keith. The DPG-Star method. *Comp. and Math. Appl.*, 79(11):3092–3116, 2020.

[6] L. Demkowicz, J. Gopalakrishnan, S. Nagaraj, and P. Sepulveda. A spacetime DPG method for the Schrödinger equation. *SIAM J. Numer. Anal.*, 55(4):1740–1759, 2017.

[7] L. Demkowicz, J. Gopalakrishnan, S. Nagaraj, and P. Sepúlveda. A spacetime DPG method for the Schrödinger equation. *SIAM J. Num. Anal.*, 55(4):1740–1759, 2017.

[8] L. Demkowicz and P. Zanotti. Construction of DPG Fortin operators revisited. *Comp. and Math. Appl.*, 2020. Special Issue on Higher Order and Isogeometric Methods.

[9] Dow Drake, Jay Gopalakrishnan, Tathagata Goswami, and Jacob Grosek. Simulation of optical fiber amplifier gain using equivalent short fibers. *Computer Methods in Applied Mechanics and Engineering*, 360(1):112698, March 2020.

[10] Dow Drake, Jay Gopalakrishnan, and Ammar Harb. Reduced test spaces for DPG methods using rectangular elements. *Computers & Mathematics with Applications*, 2017.

[11] F. Fuentes, B. Keith, L. Demkowicz, and P. LeTallec. Coupled variational formulations of linear elasticity and the DPG methodology. *J. Comp. Phys.*, 348:715–731, 2017.

[12] Jay Gopalakrishnan, Tathagata Goswami, and Jacob Grosek. Techniques for modeling fiber laser amplifiers. In Giuseppe Nicosia and Vittorio Romano, editors, *Proc. 12th International Conference on Scientific Computing in Electrical Engineering (Plenary Talk), Taormina, Sicily, Italy*. Springer, 2020.

[13] Jay Gopalakrishnan, Luka Grubišić, Jeffrey Ovall, and Benjamin Q. Parker. Analysis of FEAST spectral approximations using the DPG discretization. *Computational Methods in Applied Mathematics*, 89(321):203–228, 2020.

[14] Jay Gopalakrishnan, Martin Neumüller, and Panayot S. Vassilevski. The auxiliary space preconditioner for the de Rham complex. *SIAM J Numer Anal*, 56(6):3196–3218, 2018.

[15] Jay Gopalakrishnan and Paulina Sepúlveda. A spacetime DPG method for acoustic waves. In Ulrich Langer and Olaf Steinbach, editors, *Space-Time Methods: Applications to Partial Differential Equations*, Radon Series on Computational and Applied Mathematics, pages 129–154. De Gruyter, 2019.

[16] S. Henneking and L. Demkowicz. A numerical study of the pollution error and DPG adaptivity for long waveguide simulations. Technical Report 20, Oden Institute, December 2019.

[17] S. Henneking, J. Grosek, and L. Demkowicz. A DPG Maxwell approach for studying nonlinear thermal effects in active gain fiber amplifiers. Technical Report 17, Oden Institute, December 2019.

[18] B. Keith, S Petrides, F. Fuentes, and L. Demkowicz. Discrete least-squares finite element methods. *Comput. Methods Appl. Mech. Engrg.*, 327:226–255, 2017.

[19] B. Keith, A. Vaziri Astaneh, and L. Demkowicz. Goal-oriented adaptive mesh refinement for non-symmetric functional settings. *SIAM J. Numer. Anal.*, 57(4):1649=1676, 2019. see also ICES Report 2017/31.

[20] J. Mora and L. Demkowicz. Fast integration of DPG matrices based on tensorization. *Computational Methods in Applied Mathematics*, 19(3):523–555, 2019.

[21] S. Nagaraj. *DPG Methods for Nonlinear Fiber Optics*. PhD thesis, The University of Texas at Austin, Austin, TX 78712, April 2018. Computational Science, Engineering and Mathematics (CSEM) program.

[22] S. Nagaraj, J. Grosek, S. Petrides, L. Demkowicz, and J. Mora Paz. A 3D DPG Maxwell approach to nonlinear Raman gain in fiber laser amplifiers. *J. Comp. Phys.*, 2019. First published version available online: 9-MAR-2019 DOI information: 10.1016/j.jcpx.2019.100002.

[23] S. Nagaraj, S. Petrides, and L. Demkowicz. Construction of DPG Fortin operators for second order problems. *Comput. Math. Appl.*, 74(8):1964–1980, 2017.

[24] S. Petrides. *Adaptive multilevel solvers for the discontinuous Petrov-Galerkin method with an emphasis on high-frequency wave propagation"*. PhD thesis, The University of Texas at Austin, Austin, TX 78712, April 2019. Computational Science, Engineering and Mathematics (CSEM) program.

[25] S. Petrides and L. Demkowicz. An adaptive DPG method for high frequency time-harmonic wave propagation problems. *Comput. Math. Appl.*, 74(8):1999–2017, 2017.

[26] Paulina Ester Sepùlveda Salas. *Spacetime Numerical Techniques for the Wave and Schrödinger Equations*. PhD thesis, Portland State University, 2018.

[27] A. Vaziri, J. Mora Paz, F. Fuentes, and L. Demkowicz. High-order polygonal finite elements using ultraweak formulations. *Comput. Methods Appl. Mech. Engrg.*, 332:686–711, 2018.

[28] A. Vaziri Astaneh, B. Keith, and L. Demkowicz. On perfectly matched layers for discontinuous Petrov–Galerkin methods. *Comp. Mech.*, 63(6):1131–1145, 2018.